Energy-Weighted Acquisition of Scintigraphic Images Using Finite Spatial Filters

Raymond P. DeVito, James J. Hamill, Jon D. Treffert, and Everett W. Stoub

Siemens Gammasonics, Inc., Applied Physics and Research Group, Hoffman Estates, Illinois

Energy weighted acquisition (EWA) is a technique for improving image contrast by correcting for some of the blurring effects of Compton scattering within the patient. We outline image formation theory as it applies to energy weighting and present a pre-processing implementation that acquires images with real-number energy-dependent weighting functions of finite spatial extent. The effect of scattered radiation on quantitative accuracy, with and without EWA, is demonstrated with sheet and point sources at various depths. A planar phantom and a clinical ^{201}Tl study demonstrate enhanced contrast and edge definition. The performance of EWA in SPECT is shown by ^{99m}Tc and ^{123}I phantom studies and a clinical ^{123}I study.

J Nucl Med 30:2029–2035, 1989

Image degradation as a result of Compton scattering is of fundamental importance in scintigraphic imaging (*1,2*) inasmuch as the total flux of radiation transmitted to the detector is several times brighter than the unscattered radiation. Inclusion of all scattered flux with the primary flux reduces the contrast by unacceptable amounts, as is evidenced by the clinical failure of gamma cameras without scatter discrimination.

The solution in use for decades employs one or more energy signal discriminators that act in a cutoff manner, discarding large portions of the scattered flux exhibiting energies below that of the primary radiation, but accepting most of the primary flux of energies lying within a relatively narrow window. This is a wasteful process since every event registered in the detector carries useful information whether or not it lies in an acceptance window or has been discarded as scatter. Removal or compensation of the remaining scatter is difficult in a postprocessing operation (*3–6*) since the most relevant data, the energy response, has been discarded during image acquisition.

In this paper we develop the theoretical basis for an instrument that utilizes the information of the entire spectrum of radiation incident on the detector by way of a probabilistic weighting of both energy and spatial data. The method is applicable to planar and tomographic imaging, and permits a quantitative measure of scatter. The utility of the method is demonstrated with phantoms and clinical images.

Received Mar. 9, 1989; revision accepted July 28, 1988.

For reprints and correspondence contact: Raymond P. DeVito, Siemens Gammasonics, Inc., Applied Physics and Research Group, 2501 North Barrington Rd., Hoffman Estates, IL 60195-7372.

THEORY

Nuclear imaging systems use very few of the randomly emitted gamma rays since only those that are aligned with the aperture of the collimator are selected. This directional selection of the collimator, together with the position information of the detector, provides the imaging ability of the gamma camera system. However, not all of the gamma rays reaching the detector have their original direction preserved. In clinical imaging, a large fraction of detected gamma rays have interacted within the patient by Compton scattering. If these events were directly recorded in the image, the image would be seriously blurred. Apart from the fact that the gamma ray has passed through the collimator, the gamma camera has no information that allows the actual emission direction to be determined. The only correlative measure of possible Compton scattering is the loss of energy by the gamma ray. Because of the small energy loss corresponding to forward scattering angles (up to 50° for < 10% at 140 keV), and the finite energy resolution of the NaI(Tl), the detector cannot precisely distinguish scattered from unscattered gamma rays. While the exact nature of individual events cannot be determined, a probabilistic interpretation is possible using energy weighted acquisition (EWA).

Consider the case of the normal window acquisition method for gamma rays emitted from ^{99m}Tc. An event with a detected energy of 126.5 keV, near the lower edge of a normal ^{99m}Tc 20% window (126–154 keV) is added to the image just as strongly as if it had registered 140.5 keV, yet the rate at which the photopeak process yields events at this apparent

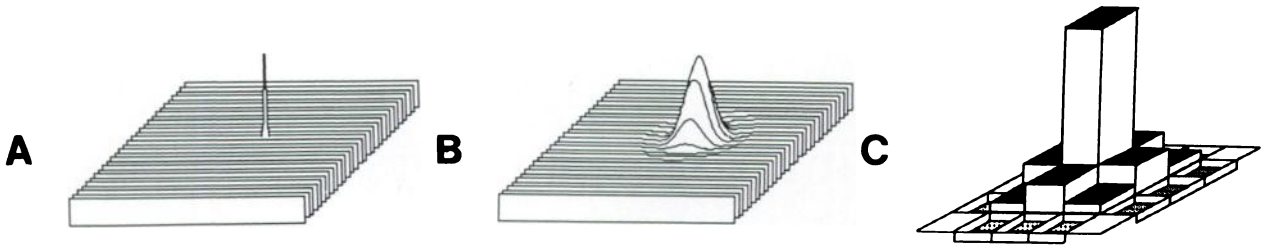

FIGURE 1
A: Impulse kernel with no spatial extent and unit value. B: Distribution kernel with finite spatial extent. C: Implementation of finite spatial kernel used in the weighted acquisition module.

energy is ~6% of the rate for 140.5 keV events, given a 10% full width at half maximum (FWHM) energy resolution. Moreover, the rate at which the scattering process yields events at this apparent energy is typically twice the rate for 140.5 keV events. Even the event recorded at 140.5 keV has a significant probability of being from a scatter process. The true source of any detected gamma ray, from either scatter or photopeak processes, cannot be determined on an event-by-event basis. However, on a probabilistic basis, the relative likelihood can be determined and used in image building. Thus, one should give 126.5 keV events less weight for photopeak image building than 140.5 keV events, and in addition one should account for the scatter probability so that the final image, statistically, has a reduction in the effects of the scatter process (*7–8*).

The effects of the scatter process tend to be diffusely distributed in position as well as in energy. The weighting functions for reducing the effects of scatter (mostly low spatial frequencies) should likewise be distributed over an area of the image surrounding the event (Fig. 1), while the strength for image building (all frequencies) should be assessed at the exact position of detection to provide maximum system resolution. The weighting functions considered in this work are energy dependent spatial filters of finite extent.

The output response, $\phi(x,y,E)$, of the camera system to a distribution of radiation, $d(x'y'z)$ in a scattering environment can be determined from the energy-dependent point-source response function (EPSRF):

$$\phi(x,y,E) = \int\int\int EPSRF(x-x',y-y',E,z)\, d(x'y'z)\, dx'dy'dz.$$

The acquisition procedure, either windowed or weighted, utilizes a weighting function, $w(x-x',y-y',E)$, to select information from the full energy dependent $\phi(x,y,E)$ and creates an image $I(x,y)$:

$$I(x,y) = \int\int\int w(x-x',y-y',E)\, \phi(x',y',E)dx'dy'dE.$$

In conventional windowed acquisition, if an event is recorded with an energy within the window, it is added to the image with a strength of +1.0 at the event coordinates. This kind of image building is represented by a weighting function that is +1.0 for energies within the window and zero outside the energy window. Furthermore, the restricted spatial extent means that the spatial kernel is represented by the Dirac delta

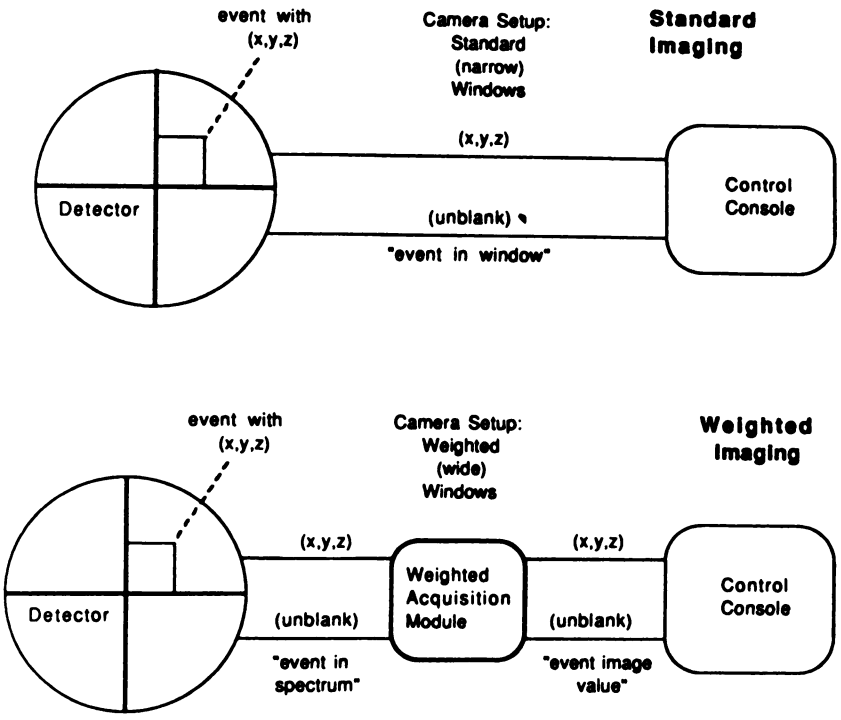

FIGURE 2
Schematic of information flow from camera to the image acquisition control console for standard imaging and for weighted imaging using the weighted acquisition module.

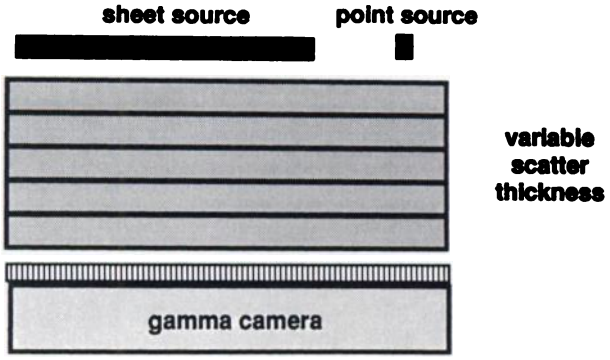

FIGURE 3
Setup for sheet source-to-point source ratio testing.

function, $\delta(x-x')$. We observe that conventional windowed acquisition is a simple subset of the general form for the weighting function $w(x-x',y-y',E)$:

$$w_{win}(x-x',y-y',E) = \delta(x-x')\delta(y-y')\,S(E),$$

where S(E) is the appropriate unit-valued step function for the desired window. Since conventional windowed acquisition is a subset of the energy weighted acquisition method, we are able to maintain overlap with all previous imaging conventions, while adding the ability to use the new method discussed here.

This weighting function depends on the detected energy of the gamma ray to the extent that the energy reflects the scatter history of the gamma ray. The degrees of freedom generated by such an approach are very large compared to the limited freedom involved in simple energy window imaging. We have developed ways to control the degrees of freedom, while maintaining the ability to significantly influence the line source response function (LSRF), especially in a scattering environment. Function generation begins with a measurement of the EPSRF. A figure of merit is defined to represent the imaging goals, for instance, the relative importance of scatter reduction compared to the signal-to-noise ratio. A gradient search is carried out to determine the weighting function that optimizes the figure of merit. Weighting functions are selected based on phantom and clinical testing. A discussion of further details of weighting function generation will be the subject of a future publication.

METHOD

We have chosen to implement the energy-dependent spatial kernels in a pre-processing configuration (*9*). This is done with a Weighted Acquisition Module (WAM) that processes event information coming from the camera and provides a standard image acquisition device with the information necessary to assemble the final processed image. Image acquisition and storage devices, such as computers and film systems, depend upon logic signals, often called unblank pulses, to indicate when an event should be recorded. Conventionally, an unblank signal was generated by the gamma camera whenever an event fell within one of the preselected energy windows. The WAM, like the gamma camera, also generates unblank pulses for image building. The WAM unblanks, produced by a new criterion, transmit more information than window acquisition methods (Fig. 2). There are actually two unblank generators in the WAM, so that each event can contribute to two images simultaneously. Two simultaneously acquired images, each processed by independent weighting functions, are available from the WAM, providing the opportunity to acquire a weighted image together with a standard window image or to directly compare two weighting functions.

The WAM contains two 128 × 128 pixel, signed, real number "read-add-write" buffer memories that allow it to track the history of events throughout the measurement and

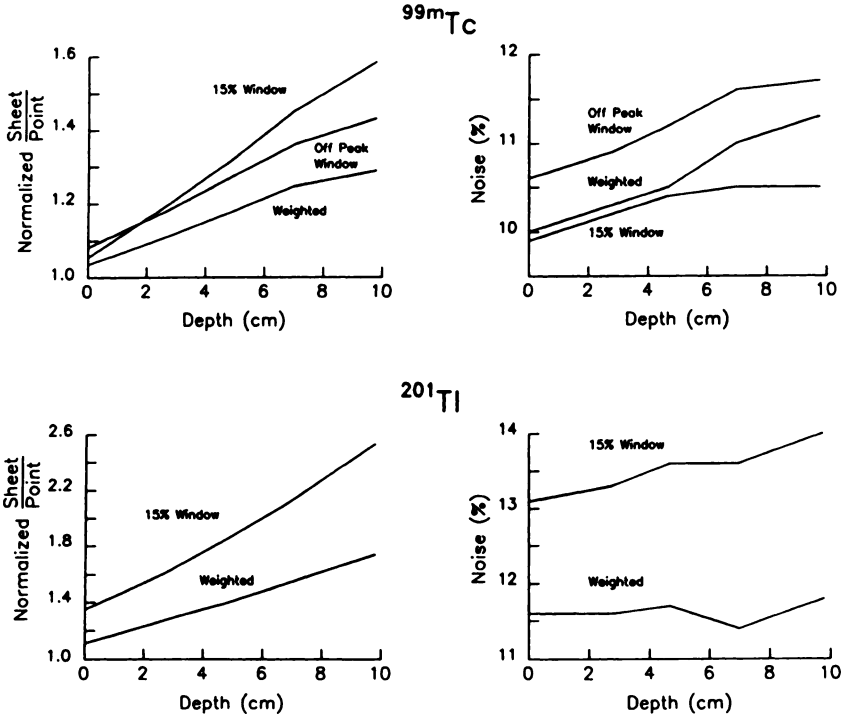

FIGURE 4
Technetium-99m and ^{201}Tl sheet-to-point ratios and standard deviation (noise) for weighted and windowed acquisitions.

provide the reference information needed to determine the image value on an event-by-event basis. By using these buffer memories, the WAM processes events with real weighting functions, yet uses unblank pulses (an integer system), for building images. The buffer memory is not used for image display, but only as an intermediate step in the image formation process. It records negative and fractional values, while the image acquisition device records positive integer values. The spatial filter is a 21 pixel kernel (a 5 × 5 region, less four corner pixels) covering an area about 16 mm in diameter for a large field of view camera (Fig. 1). This area is of a size large enough to do low amplitude, low noise scatter subtraction, as well as spatial filtering, on the scale of the system resolution.

When an event is presented to the WAM, an analog-to-digital converter (ADC) produces an accurate value for the event energy that is used for the address in the tables of weighting functions. The weighting value for the center of the kernel is added to the buffer memory pixel selected by position ADCs. The new value is then checked: if it is +1.0 or more, the integer value is removed from memory and converted into a series of one or more unblank pulses, i.e., equal to the net integer value of the event, which is emitted with the original event position coordinates and resolution. Then the weighting values for the other 20 pixels around the kernel center are added to the corresponding buffer pixels, as residual data for future reference.

The energy dependent weighting functions consist of four spatial components, corresponding to the radial distribution shown in Figure 1. Each isotope and collimator combination may require different weighting functions. The generation of weighting functions begins with a measurement of the EPSRF. A figure of merit is defined that represents the desired imaging goals, and weighting functions are generated that optimize this parameter. Various functions are possible for each isotope, depending on the needs for different imaging situations, for example; maximal scatter removal, improved signal-to-noise ratio, or edge enhancement.

RESULTS AND DISCUSSION

Phantom Studies

A simple parameterization, like the FWHM of the LSRF, is insufficient to predict the performance of a gamma camera system in the presence of a scattering medium. Phantom studies provide a more realistic measure of the system performance.

For example, quantitation requires that measurements of specific activity should be independent of the size of the lesion and independent of neighboring activity. Activities with different spatial distributions, lying at the same depth and containing the same specific activities, should yield the same counting rate per pixel. This requirement is violated when the scattered radiation is included in the measurement of the unscattered radiation. An effective scatter removal scheme allows better quantitation with less geometry dependence.

Testing this requirement at its extremes, we compared the response to very large phantoms (sheet sources) and very small phantoms (point sources). Activity of ^{99m}Tc or ^{201}Tl was loaded into a sheet source and a point source, and both sources were positioned 10 cm above a gamma camera. One part of the gamma camera viewed the sheet, while another part viewed the point. As shown in Figure 3, varying amounts of soft tissue equivalent Plexiglas were inserted between the sources and the camera. A large region of interest (ROI) under the sheet source, and a smaller ROI under the point were considered. We define a normalized sheet-to-point ratio, R, for each scatter depth:

$$R = \frac{\text{(counts in sheet ROI) / (activity above sheet ROI)}}{\text{(counts in point ROI) / (activity in point source)}}.$$

Figure 4 shows this ratio as a function of the scatter depth. The counting rates in the two ROIs fall off as more and more plexiglas is interposed, but they fall off at different rates. Much of the scattered radiation originating from the point source falls outside the small point source ROI, whereas most of the detected scattered radiation from the sheet is detected within the sheet ROI. Deviations from a constant value (ideally 1.0) indicate imperfections in the gamma camera system's ability to handle scatter. The deviations in Figure 4 follow the expected pattern, with R increasing as the amount of interposed Plexiglas increases.

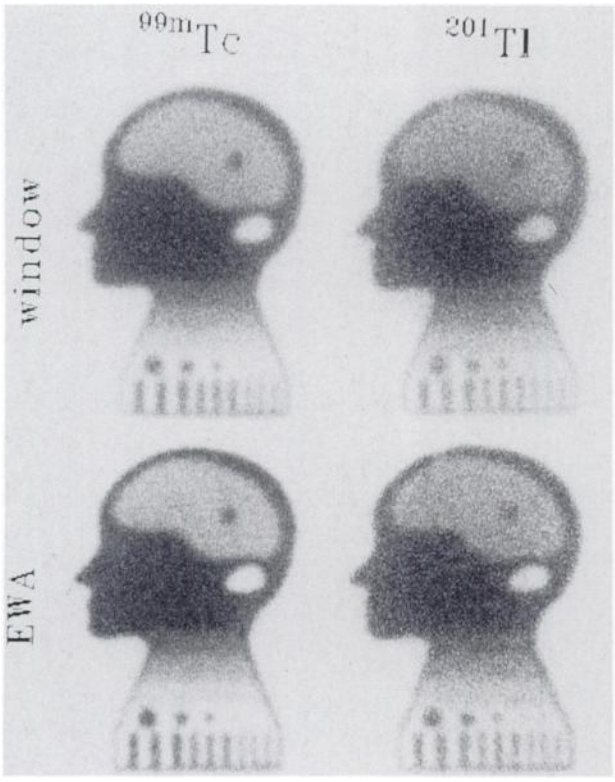

FIGURE 5
Schramm phantom images for ^{99m}Tc (right) and ^{201}Tl (left). The upper images are the normal window acquisitions and the lower images are obtained using energy weighted acquisition.

In clinical imaging, one would like to reduce the effects of scatter with as little statistical noise as possible. We calculate a noise parameter for the sheet source at each scatter depth. This parameter is defined as the root mean square (rms) percent deviation from the mean, with non-statistical source deviations subtracted in quadrature to correct for nonuniformities due solely to the source and collimator. The noise is plotted along with the sheet-to-point ratio, R, in Figure 4.

In the case of ^{99m}Tc, data was acquired with: an on-peak 15% window; an off-peak 15% window; and a weighting function. In the case of ^{201}Tl, we used: a conventional window, 20% at 74 keV and 15% at 166 keV; and a weighting function. The weighting functions used in this experiment are those that have been found to be useful from clinical investigations. For ^{99m}Tc, EWA and the off-peak window show an improved sheet-to-point ratio, but with the trade-off of increased noise. However, EWA performs better than the off-peak window in both the sheet-to-point ratio and percent rms deviation. For ^{201}Tl, no trade-off is necessary. EWA reduces both the percent rms deviation and the effects of scatter as measured in the sheet-to-point ratio.

A second, more subjective, phantom study demonstrates the loss of contrast in a simple planar imaging geometry (the Schramm phantom). Figure 5 shows

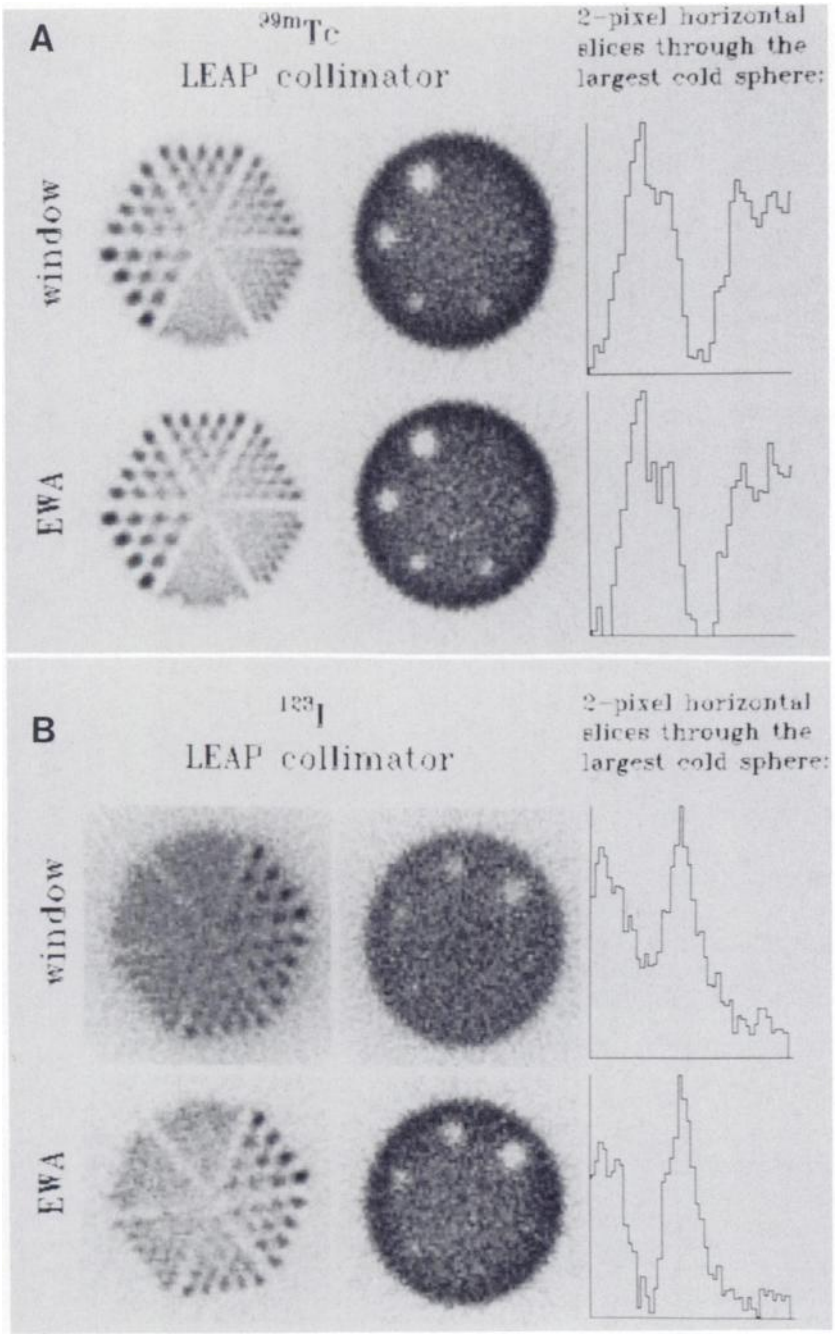

FIGURE 6
Transverse views of ECT phantom for (A) ^{99m}Tc and (B) ^{123}I. The upper images for each set are the normal window acquisitions and the lower images are obtained using energy weighted acquisition.

images obtained with normal windows and weighting functions, for ^{99m}Tc and ^{201}Tl. Both isotopes show improvement by scatter reduction. In addition to improved contrast in the areas of no activity, edge definition is improved. Examination of the deviations about the mean for various regions of this phantom shows that the window and weighted images have comparable noise characteristics. As in the sheet-to-point study, scatter is a much bigger problem for ^{201}Tl than for ^{99m}Tc. The 30 cm^2 100% cold region in this phantom, located next to a hot region, demonstrates scatter rejection. In the case of ^{201}Tl, the count density in the cold region is 40% of the count density in the hot region with windowed imaging, and is improved to 29% with energy weighted acquisition. The energy weighted acquisition technique does not exclude additional image processing when such processing is desired. Postprocessing schemes can be performed in conjunction with energy weighted acquisition (*10*) and are generally complementary to energy weighting, being neither exclusive nor competitive.

We have also investigated the use of weighted acquisition in SPECT imaging. In Figure 6, tomographic reconstruction of a SPECT phantom (Data Spectrum Phantom) are shown together with slices through a hot rod region and through a region containing cold spheres. The weighted images for ^{99m}Tc show improved contrast over the normal windowed images. The technique also works for one of the more difficult isotopes used in nuclear medicine imaging, i.e., ^{123}I contaminated with ^{124}I ("dirty iodine"). The data were taken with a low-energy, all purpose (LEAP) parallel collimator. Improved visualization of both the hot rods and the cold spheres is evident as a result of a large reduction in scatter and high-energy background. The count profile through the largest cold sphere is shown for each isotope.

Clinical Studies

Some clinical experience with energy weighted acquisition has been obtained by several investigators (*11–14*). Both planar and SPECT studies have been performed. M. D. Cooper and R. N. Beck of the University of Chicago were first to investigate the clinical application of energy weighted acquisition, using energy weighting without finite spatial kernels. Siegel et al. (*11*) acquired a set of 51 bone and gallium studies and were first to demonstrate improved contrast for weighted images compared to standard windows by quantifying the contrast for the ribs (bone) and lesions (gallium). Henkin et al. (*12*) have investigated energy weighted acquisition for ^{201}Tl myocardial planar and SPECT imaging, as well as for ^{99m}Tc and ^{67}Ga imaging (*13*). They found improved contrast in phantom and patient studies. For ^{201}Tl, the ratio of ventricular wall to chamber activity, as well as lesion edge sharpness, is improved. Examples of clinical images are shown in Figure 7.

SUMMARY AND CONCLUSION

Energy weighted acquisition using finite spatial filters has been applied in phantom and clinical studies. EWA is accomplished with the Weighted Acquisition Module, a preprocesssing device that accepts events from the gamma camera, applies the energy dependent real-valued weights on an event-by-event basis, and transforms the camera logic pulses from event flags to event value indicators. The WAM buffer memory accounts for the nonpositive-integer (negative and fractional) part of the image, while the image acquired at the image acquisition station retains the usual property of being formed from integer values only.

When scintigraphic images are contaminated by object dependent scatter, radioisotope distribution infor-

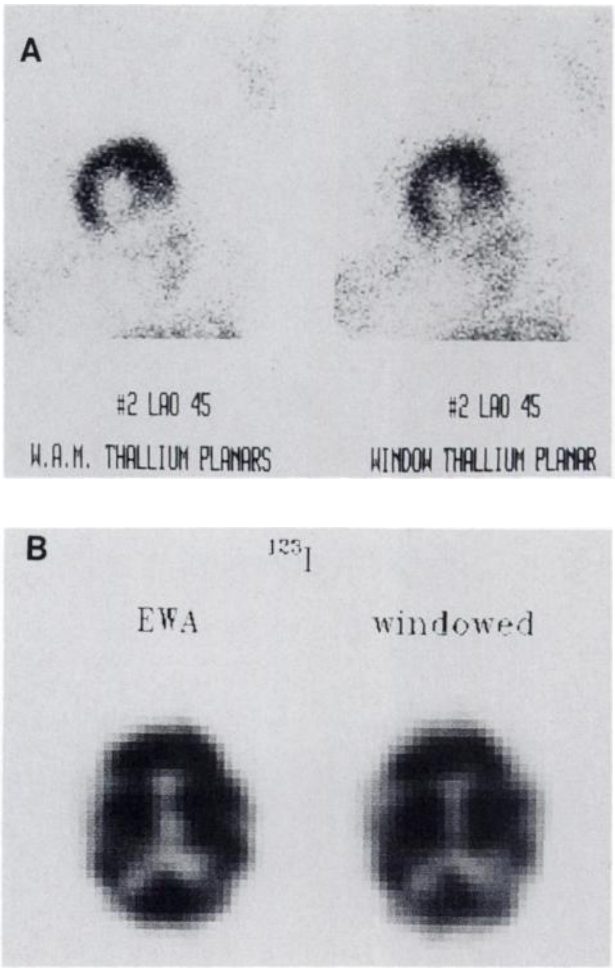

FIGURE 7
Examples of clinical images. The pairs of images were taken simultaneously. The left image of each pair is energy weighted acquisition and the right image is the normal window acquisition. A: ^{201}Tl planar view of the heart. B: ^{123}I (lofetamine) transverse SPECT view of the midbrain.

mation is degraded. Even simple planar phantoms show object-dependent scatter effects. This object dependence is demonstrated in a sheet-source to point-source ratio experiment, in which count rates for standard window acquisition techniques depend strongly on the scatter depth, while the weighted acquisition technique improves the quantitative accuracy. A more complex planar phantom demonstrates enhanced contrast and edge definition. Scatter reduction is demonstrated for ^{99m}Tc and ^{201}Tl, with the latter suffering greater losses in contrast and ability to quantitate because of scatter. SPECT phantom studies show promising results, even for isotopes with high energy contamination problems ("dirty" ^{123}I). Clinical experience shows improved images for both planar and SPECT imaging.

EWA provides a way to utilize previously discarded information in nuclear medicine imaging. Although a new technique, it incorporates the accepted windowed acquisition technique as a special subset of weighting functions. Weighted acquisition is a practical technique that effectually addresses the problem of Compton scatter.

ACKNOWLEDGMENTS

The authors thank Dr. R.E. Henkin of Loyola University for the clinical ^{201}Tl images, Dr. R.E. Coleman of Duke University for the clinical ^{123}I images, and Mr. Orest Zabrodsky for technical assistance.

REFERENCES

1. Ehrhardt JC, Oberley LW, Lensink SC. Effect of a scattering medium on gamma ray imaging. *J Nucl Med* 1974; 15:943–948.
2. Dimitriou P, Tzimas J, Tsialas S. Effect of scatter radiation on the planar source sensitivity of a collimated detector. *Eur J Nucl Med* 1984; 9:229–232.
3. La Fontaine R, Stein MA, Graham LS, Winter J. Cold lesions: enhanced contrast using asymmetric photopeak windows. *Radiology* 1986; 160:255–260.
4. Jaszczak RJ, Greer KL, Floyd, Jr. CE, Harris CC, Coleman RE. Improved SPECT quantification using compensation for scatter photons. *J Nucl Med* 1984; 25:893–900.
5. Oppenheim BE. Scatter correction for SPECT. *J Nucl Med* 1984; 25:928–929.
6. Msaki P, Axelsson B, Dahl CM, Larsson SA. Generalized scatter correction method in SPECT using point scatter distribution functions. *J Nucl Med* 1987; 28:1861–1869.
7. Beck RN, Zimmer LT, Charleston DB, Hoffer PB. Aspects of imaging and counting in nuclear medicine using scintillation and semiconductor detectors. *IEEE Trans Nucl Sci* 1972; 19:173–178.
8. Beck RN, Zimmer LT, Charleston DB, et al. Advances in fundamental aspects of imaging systems and techniques. In: *Medical radioisotope scintigraphy.* Vol. I. Vienna: IAEA 1973; 3–45.
9. Hamill JJ, DeVito RP. Scatter reduction with energy weighted acquisition. *IEEE Trans Nucl Sci* 1989; 36:1334–1339.
10. DeVito RP, Treffert JD, Hamill JJ, Jaszczak RJ. Scatter removal by pre- and post-processing techniques [Abstract]. *J Nucl Med* 1988; 29:798.
11. Siegel ME, Lee KH, DeVito RP, Chen O, Chen DCP. Weighted acquisition: A method for improving bone and gallium images [Abstract]. *J Nucl Med* 1986; 27: 988.
12. Henkin RE, Halama JR, Friend LE, Dillehay GL, Schultz KR, DeVito RP. Improved gamma camera imaging with energy weighted acquisition [Abstract]. *J Nucl Med* 1987; 28:758.
13. Halama JR, Henkin RE, Friend LE. Gamma camera radionuclide images: improved contrast with energy weighted acquisition. *Radiology* 1988; 169:533–538.
14. Murphy PH, Long SE, Moore WH, Dhekne RH, Blust MJ, Pounds BK. Improved image contrast by scatter suppression with energy weighted acquisition [Abstract]. *J Nucl Med* 1988; 29:1316.